


Improvements to the stochastic series expansion method for the JQ_2 model with a magnetic field

Lu Liu ^{*}

School of Physics, Beijing Institute of Technology, Beijing 100081, China

 (Received 31 October 2023; revised 8 January 2024; accepted 10 January 2024; published 22 January 2024)

The stochastic series expansion (SSE) quantum Monte Carlo method with directed loops is very efficient for spin and boson systems. The Heisenberg model and its generalizations, such as the JQ_2 model, are extensively simulated via this method. When introducing magnetic field in these models, the SSE method always combines the field with the diagonal part of the Heisenberg interactions ($S_i^z S_j^z$) and take them as the new diagonal operators. In general, this treatment is reasonable. However, when studying Hamiltonians, which have other interactions or even do not contain the Heisenberg interactions, this general treatment will not be efficient or even not work. We suggest that when doing directed-loop simulations, the magnetic field can be put into other interactions. This treatment, in some cases, improves the simulation efficiency. Using the JQ_2 model with magnetic field as an example, we here demonstrate this SSE method. Such treatment significantly improves the efficiency when the Q_2 interactions are large. The autocorrelations are reduced a lot compared to the previous approach. In addition, we argue that we can divide the magnetic field into two parts and combine them with both the J and Q operators respectively. This treatment also improves the simulation efficiency. The underlying mechanism is that these two SSE methods can utilize the main part or even all part of operators in operator products to do the directed-loop updates. Such idea can also be applied to other models with magnetic field and it will speed up the simulations.

DOI: [10.1103/PhysRevB.109.045141](https://doi.org/10.1103/PhysRevB.109.045141)

I. INTRODUCTION

The stochastic series expansion (SSE) quantum Monte Carlo (QMC) method [1] with loop update [2–4] is a very powerful method for quantum spin systems and boson systems. The Heisenberg model and its generalizations (e.g., the JQ models) are extensively simulated by this method. When introducing magnetic field, Syljuåsen and Sandvik proposed SSE method with directed-loop update, which includes the field operators into the Heisenberg interactions [4]. The Heisenberg model is taken as a specific example to demonstrate that the directed-loop simulations are very efficient for the full range of magnetic field (zero to the saturation point). When simulating the generalizations of the Heisenberg model, which not only contain the Heisenberg interactions but also have other interactions, people in general still combine the magnetic field with the Heisenberg interactions [5–7]. Such treatment does work for most cases. However, it is not the most efficient way for some extreme cases. In this paper, we argue that not only can the Heisenberg interaction be combined with the external magnetic field, but also other interactions can contain the magnetic field. The simulations, in some cases, are more efficient when we put the magnetic operators into other interactions. What is more, we can divide the magnetic field and combine them with all the types of interactions. In this paper, we consider the JQ_2 model with magnetic field as a specific example. We present that the two

versions of the SSE method with directed loops are more efficient than that of the general SSE method when Q is large.

This paper proceeds as follows. In Sec. II, backgrounds on the JQ_2 model are given. In Sec. III, we introduce the basic concepts of the SSE method. In Sec. IV, we briefly review the general SSE method with directed loops for the JQ_2 models with an external magnetic field. In Sec. V, we present our two versions of the SSE methods for the JQ_2 model with magnetic field. In Sec. VI, we present simulation results and show that the two versions of the SSE method do work and decrease the autocorrelation times significantly. We conclude in Sec. VII.

II. THE JQ_2 MODEL

The JQ_2 model is a generalization of the Heisenberg model, which has four-spin interactions Q on every plaquette. The Hamiltonian is expressed as

$$H = -J \sum_{\langle ij \rangle} P_{ij} - Q \sum_{\langle ij, kl \rangle} P_{ij} P_{kl} = -(H_J + H_Q) \quad (1)$$

where $P_{ij} = 1/4 - \mathbf{S}_i \cdot \mathbf{S}_j$ is the singlet projector operator, $\langle ij \rangle$ represent two nearest-neighbor sites, $\langle ij, kl \rangle$ represents four sites on one plaquette and the index pairs ij, kl form two parallel bonds on horizontal or vertical directions. The summations are over all nearest neighbors for the J terms and all translations of the vertical and horizontal stacks for the Q terms. H_J and H_Q stand for the J and Q terms in the Hamiltonian. In this paper, we take $J = 1$ as the unit of energy. We call every interaction as a bond and the JQ_2 model has two types of bonds: the J bonds and Q bonds. This model was proposed by Sandvik to show the deconfined quantum

^{*}liulu96@bit.edu.cn

phase transition from the Néel state to the valence-bond-solid (VBS) state [8] and later other variants of the JQ models were proposed, such as the JQ_n model (the JQ_n model means every Q operator is the products of n singlet projector operators), the checkerboard JQ ($CBJQ$) model. Lots of novel properties were found in these models. In the JQ_3 model, there also exists the deconfined quantum phase transition [9]; there is a symmetry enhanced first-order phase transition in the $CBJQ$ model [10]; in the JQ_6 model, an emergent $SO(5)$ symmetry was observed [11]; in a modulated- JJQ model, the multi-critical deconfined quantum criticality was found [12].

There is a deconfined quantum phase transition in the JQ_2 model. When $g = J/Q$ is large, the ground state is the Néel state and when $g = J/Q$ is small enough, the ground state is the VBS state. The transition point between these two phases is $g_c = J/Q \approx 0.045$, which means when we set $J = 1$, the value of Q_c will be around 22 [13]. Such value is really large. When we are interested in the properties of the JQ_2 model around Q_c or the properties of VBS state, we have to set Q very large. The SSE method is efficient for the simulations of this model. However, when introducing an external magnetic field, the situation will be different. We find the general SSE method with directed loops, where the magnetic field is combined with the Heisenberg interactions (J terms), is less efficient. The autocorrelation time is much longer and we need very large Monte Carlo steps to obtain high-quality data. When the system size and inverse temperature increase, the autocorrelation time will increase significantly and we can even not get the correct results because of the limitation of computational resources. An intuitive idea is that for the JQ_2 model without external field, the average number of times that the operators of the J (Q) bonds appearing in the operator string is proportional to the expectation value of H_J (H_Q). When Q is much larger than J , the expectation value of H_Q will also be much larger than that of H_J . It means the Q bonds occur more frequently than the J bonds in the operator strings (see Appendix B). When introduced magnetic field, the general directed-loop update only makes use of the small part (J bonds) of the operator strings, which of course is not efficient. In this article, we propose that we can use the main part of the operator string (Q bonds) to do the directed-loop updates or we can use all the bonds in the operator strings (both J and Q bonds) to do the directed-loop updates. The two treatments reduce the autocorrelation time significantly and make the simulations more efficient.

In the next two sections, we will introduce the general concepts of SSE method and talk about the general treatment of the JQ_2 model with magnetic field in the SSE method.

III. BASIC CONCEPTS OF SSE METHOD

In this section, we will introduce some basic concepts of the SSE method.

For general models with N spins, such as the Heisenberg antiferromagnet and the JQ model, we use the standard basis for these models

$$|\alpha\rangle = |S_1^z, S_2^z, \dots, S_N^z\rangle \quad (2)$$

and write the Hamiltonians in terms of bond operators H_b ,

$$H = - \sum_{b=1}^{N_b} H_b \quad (3)$$

where every index b refers to one interaction term: for the Heisenberg interactions, one bond only contains two spins and for multispin interactions, such as Q terms in the JQ model, one Q bond can contain more spins. N_b is the number of bonds. In order to carry out the SSE simulations, we need divide every bond into \mathbb{N} operators,

$$H_b = H_{1,b} + \sum_{i=2}^{\mathbb{N}} H_{i,b} \quad (4)$$

where $H_{1,b}$ is the diagonal part of bond operator and $H_{i,b}$ ($i \geq 2$) are the off-diagonal bond operators. We will see that for the Heisenberg interaction $\mathbb{N} = 2$ and for the Q_n interaction $\mathbb{N} = 2^n$ (the Q_2 interactions $\mathbb{N} = 4$; the Q_3 interactions, $\mathbb{N} = 8$). The definition of the JQ model has been shown in Sec. II.

The starting point of the SSE method is the Taylor expansion of the partition function,

$$Z = \text{Tr}\{e^{-\beta H}\} = \sum_{\alpha} \sum_{n=0}^{\infty} \frac{(-\beta)^n}{n!} \langle \alpha | H^n | \alpha \rangle \quad (5)$$

where the trace is written as summation of basis $|\alpha\rangle$ and $\beta = 1/T$ is the inverse temperature. Next, according to Eq. (4), the operator string H^n need to be expanded as summations of products of diagonal and off-diagonal bond operators. We truncate the expansion power n at a maximum value M and then fix the operator products length as M by introducing some unit operators. For general expansion power n ($n \leq M$), we need insert $M - n$ unit operators $H_{0,0} = I$ in the operator products in all possible ways. Finally, the partition function is written as

$$Z = \sum_{\alpha} \sum_{S_M} \frac{\beta^n (M - n)!}{M!} \langle \alpha | \prod_{i=1}^M H_{a_i, b_i} | \alpha \rangle \quad (6)$$

where n is the number of nonunit bond operators, $a_i = 1, 2, \dots, \mathbb{N}$ corresponds the type of operators (0, unit; 1, diagonal; 2, 3, \dots , off-diagonal) and $b_i = 0, 1, 2, \dots, N_b$ is the bond index (0 for unit operators, 1, 2, \dots, N_b for nonunit bonds). S_M is the configurations of operator products. Such a product can be referred to by an operator-index sequence

$$S_M = [a_1, b_1], [a_2, b_2], \dots, [a_M, b_M]. \quad (7)$$

For simplicity, we sometimes use the notation $[a, b]_p$ to represent $[a_p, b_p]$, where p can be thought as the index of imaginary time.

One can show that the average expansion order is

$$\langle n \rangle = \beta |E| \quad (8)$$

where E is the system energy, $E = \langle H \rangle$ [3,4]. The width of the expansion order is approximately $\langle n \rangle^{1/2}$. The cutoff M can be chosen so that n can never reaches this value. The truncation error is then negligible.

The Monte Carlo simulation can be started with some random state $|\alpha\rangle$ and “unit” operator string $S_M = [0, 0]_1, [0, 0]_2, \dots, [0, 0]_M$. The general SSE sampling of

configurations (α, S_M) contains two different types of updates, which ensure the ergodicity of the sampling. The first update (diagonal update) is of the update between the unit operator $[0, 0]_p$ and the diagonal operator $[1, b]_p$. Such update will change the expansion order n by ± 1 . The corresponding Metropolis acceptance probabilities are

$$P([0, 0]_p \rightarrow [1, b]_p) = \min \left\{ 1, \frac{N_b \beta \langle \alpha(p) | H_{1,b} | \alpha(p) \rangle}{M - n} \right\}, \quad (9)$$

$$P([1, b]_p \rightarrow [0, 0]_p) = \min \left\{ 1, \frac{M - n + 1}{N_b \beta \langle \alpha(p) | H_{1,b} | \alpha(p) \rangle} \right\}. \quad (10)$$

The second update (off-diagonal update) is of the update between the diagonal operators $[1, b]_p$ and the off-diagonal operators $[a, b]_p$, where $a \geq 2$. It can be done by the loop update. Readers can refer to article [3,4] for detail information about the off-diagonal update for the Heisenberg model. These two SSE methods introduced in this paper have the same update processes, which also contain both the diagonal update and the off-diagonal update.

It is convenient to define a Monte Carlo step (MCS) for the SSE simulation. One MCS contains a sweep of diagonal updates at all imaginary time positions and then do the construction of linked list. After this construction, a fixed number of loop updates are applied. Thus every MCS contains both types of updates.

During the simulation, we should firstly evolve the initial configuration to the equilibrated configurations and then the reliable measurements are possible. Thus in Monte Carlo simulations, one firstly do some ‘‘equilibration’’ MCSs and then do some ‘‘measure’’ MCSs. The number of these two MCSs depends on the equilibrium correlation time and the autocorrelation time; we will not discuss this in detail. The physical observables are measured during the ‘‘measure’’ MCSs. A general observable A (mostly diagonal observables) can be measured according to

$$\begin{aligned} \langle A \rangle &= \frac{1}{Z} \sum_{\alpha, S_M} \frac{\beta^n (M - n)!}{M!} \langle \alpha | A \prod_{i=1}^M H_{a_i, b_i} | \alpha \rangle \\ &= \sum_{\alpha, S_M} A(\alpha, S_M) W(\alpha, S_M) / \sum_{\alpha, S_M} W(\alpha, S_M) \end{aligned}$$

where

$$\begin{aligned} A(\alpha, S_M) &= \frac{\langle \alpha | A \prod_{i=1}^M H_{a_i, b_i} | \alpha \rangle}{\langle \alpha | \prod_{i=1}^M H_{a_i, b_i} | \alpha \rangle}, \\ W(\alpha, S_M) &= \frac{\beta^n (M - n)!}{M!} \langle \alpha | A \prod_{i=1}^M H_{a_i, b_i} | \alpha \rangle. \end{aligned}$$

We will not discuss the measurement in detail here. Several observables have been derived in Refs. [3,14]. The off-diagonal correlation functions have been studied in Ref. [15].

IV. GENERAL SSE METHOD FOR THE JQ_2 MODEL WITH MAGNETIC FIELD

In this section, we introduce the general SSE method that deals with the magnetic field in the JQ_2 model. The

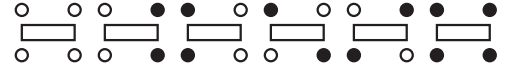


FIG. 1. 6 different vertices for the J operators. The horizontal bar represents the operators. The circles beneath (above) represent the spin state (open and solid circles for spin- \uparrow and spin- \downarrow , respectively) before (after) operation with the J operators. We denote these six vertices as Γ_i , $i = 1, 2, 3, 4, 5, 6$. We denote the four circles as four legs of the vertex.

Hamiltonian of the JQ_2 model can be written as

$$H_{JQ_2-h} = - \sum_{\langle ij \rangle} J P_{ij} - \sum_{\langle ij, kl \rangle} Q P_{ij} P_{kl} - h \sum_i S_i^z. \quad (11)$$

The last term in Eq. (11) is the magnetic field. When doing the SSE simulations on this model, we generally put the magnetic field into the diagonal part of the J terms. In order to ensure all matrix elements of the new diagonal part of the J terms are not negative, we also need to add a constant. Such constant is not unique, people can choose any value as long as the diagonal part of the J terms have no negative matrix elements. The final Hamiltonian of the JQ_2 model with magnetic field is written as

$$\begin{aligned} H_{JQ_2-h} &= - \sum_{\langle ij \rangle} J(P_{ij} + h_b(S_i^z + S_j^z + 1) + \epsilon) \\ &\quad - \sum_{\langle ij, kl \rangle} Q P_{ij} P_{kl}. \end{aligned} \quad (12)$$

In Eq. (12), we have defined the magnetic field on a J bond, the field strength is $h_b = h/zJ$ and z is the coordination number. In addition, we have added a constant $h_b + \epsilon$ on every J bond and $\epsilon \geq 0$.

When doing the SSE simulations, we divided every J term in Eq. (12) into two operators: one is diagonal $H_{ij}^{(1)} = 1/4 - S_i^z S_j^z + h_b(S_i^z + S_j^z + 1) + \epsilon$ and the other is off-diagonal $H_{ij}^{(2)} = -(S_i^x S_j^x + S_i^y S_j^y) = -1/2(S_i^+ S_j^- + S_i^- S_j^+)$. Every matrix element of these two types of operators can be represented by a vertex and they will give six different vertices. We denote these vertices as Γ_i ($i = 1, 2, 3, 4, 5, 6$). The six different vertices contain four diagonal vertices and two off-diagonal vertices (In diagonal vertices, the spin state does not change after the operation of an operator. In the off-diagonal vertices, the spin state will change after the operation of an operator). The four diagonal vertices are $\Gamma_1 : \langle \uparrow \uparrow | H^{(1)} | \uparrow \uparrow \rangle$, $\Gamma_2 : \langle \uparrow \downarrow | H^{(1)} | \uparrow \downarrow \rangle$, $\Gamma_3 : \langle \downarrow \uparrow | H^{(1)} | \downarrow \uparrow \rangle$, $\Gamma_6 : \langle \downarrow \downarrow | H^{(1)} | \downarrow \downarrow \rangle$ and the two off-diagonal vertices are $\Gamma_4 : \langle \uparrow \downarrow | H^{(2)} | \downarrow \uparrow \rangle$, $\Gamma_5 : \langle \downarrow \uparrow | H^{(2)} | \uparrow \downarrow \rangle$. The index of these six vertices can be set arbitrarily. The weight of these six vertices (matrix element of operators) are $W(\Gamma_1) = 2h_b + \epsilon$, $W(\Gamma_2) = 1/2 + h_b + \epsilon$, $W(\Gamma_3) = 1/2 + h_b + \epsilon$, $W(\Gamma_4) = 1/2$, $W(\Gamma_5) = 1/2$, $W(\Gamma_6) = \epsilon$ respectively. These vertices are shown in Fig. 1.

Every Q_2 term contains a product of two singlet projector operators. In the SSE simulations, it also should be divided. As every singlet projector operator P_{ij} can be divided into two part: one is diagonal $H_{ij}^{(1)} = 1/4 - S_i^z S_j^z$ and the other is off-diagonal $H_{ij}^{(2)} = -1/2(S_i^+ S_j^- + S_i^- S_j^+)$. Note that the diagonal operator $H^{(1)}$ here, which does not contain magnetic field part, is different from the diagonal operator of J terms

mentioned above. However, we denote both of them as $H^{(1)}$ for simplicity. Thus for every Q_2 term, it can be divided into four different operators: $H_1 = H_{ij}^{(1)}H_{kl}^{(1)}$, $H_2 = H_{ij}^{(1)}H_{kl}^{(2)}$, $H_3 = H_{ij}^{(2)}H_{kl}^{(1)}$, and $H_4 = H_{ij}^{(2)}H_{kl}^{(2)}$. H_1 is the diagonal part of the Q operator and the three others are off-diagonal parts of the Q operator. Every off-diagonal term of the Q_2 operators has at least one $H^{(2)}$. We denote these four terms as $H_1 = Q_{ijkl}^{(11)}$, $H_2 = Q_{ijkl}^{(12)}$, $H_3 = Q_{ijkl}^{(21)}$, $H_4 = Q_{ijkl}^{(22)}$.

For JQ_2 model with magnetic field, every diagonal part of the J operators contains the field and every diagonal part of the Q operators does not contain any magnetic field. Thus when doing the diagonal update, the weight for the J diagonal operators should include the field operators. The off-diagonal update is a bit complicated. When a loop encounters the J operators, the loop should choose the exit leg with a probability, which corresponds to the particular solution of the directed-loop equations {see Eqs. (29) and (31) in Ref. [4]}. When the loop encounters the Q operators, it will just do the simple switch-and-reverse moves. This treatment introduced above is the general SSE method. In the next section, we will present a modified version of SSE method for the JQ_2 model with magnetic field.

V. MODIFIED VERSION OF SSE METHOD FOR THE JQ_2 MODEL WITH MAGNETIC FIELD

As mentioned above, the critical point Q_c is really large for the JQ_2 model. When Q is large, the J operators appear much less frequently than the Q operators. If we study the properties of the JQ_2 model at large Q with external magnetic field, we will find the efficiency of the general SSE method with directed loops is very poor and we suggest a modified version of the SSE method, which is more efficient.

As the operators appearing in the operator products will mostly be the Q operators, if we can do the SSE simulations by combining the Q operators and magnetic field together, the simulations is more efficient than the general SSE method. In this section we will show such combination can indeed be applied in the SSE method. What is more, if we only combine the magnetic field with the Q operators, the directed-loop updates only make use of the Q operators. The J operators do not participate in the directed-loop updates. When a loop encounters the J operators, it just does the switch-and-reverse moves. We argue that the magnetic field can be divided into two parts. The first part is combined with the J operators (just as the general method) and the second part is combined with the Q operators. Any proportion of the division works for the SSE method, but the best proportion depend on the parameters (the strength of the J and the Q interactions). As all nonunit operators will take participate in the directed-loop updates, it speed up the simulations much more if the proportion of division is chosen properly. In order to distinguish these three different SSE methods, we denote the general SSE method as “J-SSE” (the directed loops only work on the J operators). The modified SSE method, in which the magnetic field is combined with the Q operators, is denoted as “Q-SSE”. The final modified SSE method, in which the magnetic field is split and combined to both J and Q operators, is denoted as

“JQ-SSE”. The J-SSE and Q-SSE method can be thought as two extreme cases of JQ-SSE method.

In this section, we present how to combine the magnetic field with the Q operators in the modified Q-SSE and JQ-SSE methods. We then show how to do the simulations in the Q-SSE method. The correctness of the Q-SSE method will be proven in the next section by comparing the results of the Q-SSE method with the exact diagonalization (ED) method.

The Hamiltonian of the JQ_2 model with magnetic field can also be written as

$$H'_{JQ_2-h} = - \sum_{(ij)} JP_{ij} - \sum_{(ij,kl)} Q(P_{ij}P_{kl} + h_q(S_i^z + S_j^z + S_k^z + S_l^z))$$

where have defined the magnetic field on a Q bond and the strength is $h_q = h/2zQ$.

We then put the magnetic field term $h_q(S_i^z + S_j^z + S_k^z + S_l^z)$ into the diagonal part of the Q_2 operator: $Q_{ijkl}^{(11)}$. The diagonal part now is written as

$$Q_{ijkl}^{(11)} = H_{ij}^{(1)}H_{kl}^{(1)} + h_q(S_i^z + S_j^z + S_k^z + S_l^z).$$

In order to make all matrix elements (vertices weight) not negative for the diagonal part of the Q operators, we also need to add a constant as that in the traditional SSE method (J-SSE) for the diagonal part of the J operators. The constant we choose in this paper is $2h_q$ for every Q bond and of course this constant is also not unique. People can choose another constant and the principle of derivation is the same. The constant $2h_q$ chosen here corresponds to $\epsilon = 0$ for the J-SSE method. In this paper, we choose $\epsilon = 0$ for the J-SSE method and JQ-SSE method in order to focus on the efficiency difference when combining the magnetic fields with different types of operators. Finally, the diagonal part of the Q_2 operators is written as

$$Q_{ijkl}^{(11)} = H_{ij}^{(1)}H_{kl}^{(1)} + h_q(2 + S_i^z + S_j^z + S_k^z + S_l^z).$$

In our simulations, the final Hamiltonian now is written as

$$H_{JQ_2-h} = - \sum_{(ij)} J(H_{ij}^{(1)} + H_{ij}^{(2)}) - \sum_{(ij,kl)} Q(Q_{ijkl}^{(11)} + Q_{ijkl}^{(12)} + Q_{ijkl}^{(21)} + Q_{ijkl}^{(22)}) \quad (13)$$

where $H_{ij}^{(1)} = 1/4 - S_i^z S_j^z$, $H_{ij}^{(2)} = -1/2(S_i^+ S_j^- + S_i^- S_j^+)$ and $Q_{ijkl}^{(11)} = H_{ij}^{(1)}H_{kl}^{(1)} + h_q(2 + S_i^z + S_j^z + S_k^z + S_l^z)$, $Q_{ijkl}^{(12)} = H_{ij}^{(1)}H_{kl}^{(2)}$, $Q_{ijkl}^{(21)} = H_{ij}^{(2)}H_{kl}^{(1)}$, and $Q_{ijkl}^{(22)} = H_{ij}^{(2)}H_{kl}^{(2)}$.

As every Q operator can be thought as the product of two J bonds, thus every Q operator will give $36 = 6 \times 6$ different types of vertices: 16 of them are diagonal, 20 of them are off-diagonal. Every vertex of the Q bond acts on 4 sites and has 8 legs. The 36 kinds of vertices are shown in Fig. 2. The 16 kinds of diagonal vertices are shown in blue regions and the 20 kinds of off-diagonal vertices are shown in white region. In the Q-SSE method, there are two same types of updates as that of the J-SSE method. The first update (diagonal update) is the same as the general one, where only the weight are changed. The weights of the J vertices do not contain the magnetic

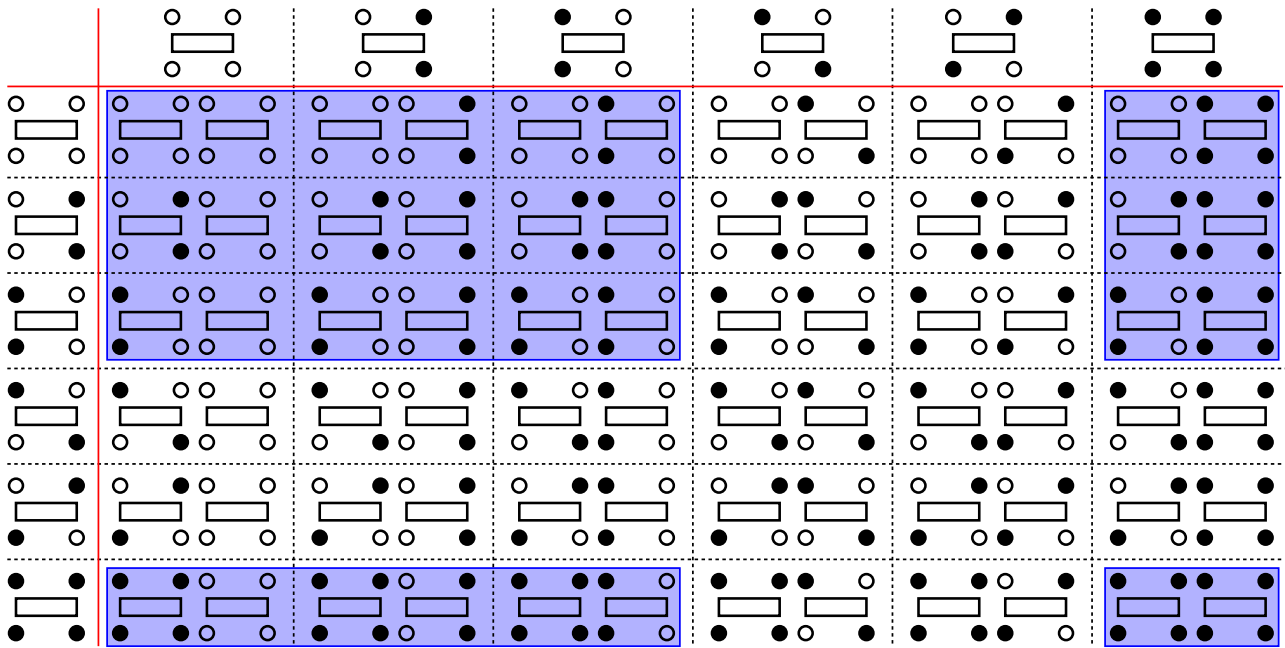


FIG. 2. $36 = 6 \times 6$ types of vertices for the Q_2 operators. The diagonal vertices are shown in blue regions and the others are off-diagonal vertices.

field and instead the weights of the Q vertices contain the magnetic field. The weights for the Q operators, which have 36 kinds of vertices, are shown in Fig. 3. In this figure, we just show the absolute value of weight and ignore the minus sign that may appear in the matrix elements of off-diagonal operators. This is because for the JQ_2 model in bipartite lattice, the number of the off-diagonal operators with negative weight is required to be even in every allowed configuration in the SSE method, in order to satisfy the “imaginary time”

periodicity (it is just the requirement of the trace of the partition function) [3].

The second update is also the directed-loop update (off-diagonal update) but it will be different from the J-SSE method. When a loop encounters the J operators, it will just do the switch-and-reverse move. However, when the loop encounters the Q operators, we need solve the directed-loop equations for the Q operators and using these solutions to do the directed-loop update.

	4hq	3hq	3hq	0	0	2hq
	3hq	$1/4+2hq$	$1/4+2hq$	1/4	1/4	hq
	3hq	$1/4+2hq$	$1/4+2hq$	1/4	1/4	hq
	0	1/4	1/4	1/4	1/4	0
	0	1/4	1/4	1/4	1/4	0
	2hq	hq	hq	0	0	0

FIG. 3. The weight of $36 = 6 \times 6$ types of vertices for the Q_2 operators. The diagonal vertices are shown in blue regions and the others are off-diagonal vertices.

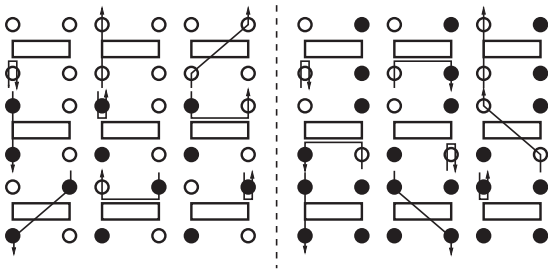


FIG. 4. Two independent assignments of directed-loop segments for every column in Fig. 2. All other directed-loop segments can be derived from these two segments by certain symmetry transformation. The lines with arrows are the directed loops and the arrows present the direction of loops.

The updates for the JQ-SSE method are similar. As both the J and Q operators contain the magnetic field, the weights for the diagonal J and Q operators should contain part of magnetic field that are assigned to these operators. The first update (diagonal update) is the same as previous and only the weights are different. However, for the second update (directed-loop update), both J and Q operators should do the directed-loop update based on the solutions of the directed-loop equations for J and Q cases. The solutions for the J operators can be found in Eqs. (29) and (31) in Ref. [4] and the solutions for the Q operators will be shown later in this section.

In Fig. 2 we have shown all the types of the Q vertices. Every Q vertex can be thought of containing left vertex and right vertex. Both vertices (left vertex and right vertex) are similar to the J vertices. Because of symmetry reasons (spins/bonds permuting and imaginary time inversion), we only need to consider the loop appearing on the left vertex. If the loop appears on the left vertex, there are two independent sets of directed-loop equations for every type of right vertex. These two sets of equations are similar to the equations appearing in the J-SSE method. As the right vertex has six different types, the total number of independent sets of directed-loop equations is $2 \times 6 = 12$. We have not excluded the cases, which vertices weight are zero. The weights of these vertices may not be zero if we choose another constant rather than $2h_q$.

Now we try to solve these 12 sets of equations. For every column in Fig. 3, there are two independent assignments of directed-loop segments, as shown in Fig. 4. These two assignments correspond two independent sets of directed-loop equations. All other assignments can be derived from these two assignments by certain symmetry transformation. Every set of equations should obey

$$\sum_x W(s, e, x) = W_s \quad (14)$$

where s denotes the configuration of a vertex, which has a weight W_s . $W(s, e, x) \equiv W_s P(s, e \rightarrow s', x)$, e is the entrance leg of the vertex and x is the exit leg of the vertex. $P(s, e \rightarrow s', x)$ means that if the entrance leg is e in a vertex with a configuration s , the loop will exit the vertex from leg x with a probability $P(s, e \rightarrow s', x)$. s' is the new configuration of this vertex after the loop going through this vertex.

According to Eqs. (14), we can get the corresponding directed-loop equations for every set and the solutions can be derived easily. Note that every set of directed-loop equations has an infinite number of solutions, the solution shown below is particular: we minimize the bounce probability (the entrance leg and exit leg are the same). Such idea is based on the intuitive hypothesis (we have no rigorous proof) that minimizing the bounce probability will increase the simulation efficiency. It can not be ruled out that there exists a more efficient directed-loop solution in which the bounce probability is not minimized.

Now we present the solutions of all the 12 sets of equations with minimized bounce probability. We will show how to solve the directed-loop equations step-by-step in Appendix A. Firstly, we present the solutions of the two sets of equations for the first column in Fig. 3, where the right vertex is Γ_1 . The left assignments of directed-loop segments, shown in Fig. 4, give the first set of equations,

$$4h_q = b_1 + a + b, \quad 3h_q = a + b_2 + c, \quad 0 = b + c + b_3, \quad (15)$$

where the left-hand sides are the vertex weights in the spin configuration space and those on the right are weights in the enlarged configuration space of spins and directed-loop segments. The probabilities of selecting the exit leg are dividing the weights in the extended configuration space by the weight of the bare vertex (spin configuration space). For example, if the loop encounters a vertex Γ_1 and the entrance leg is the lower left leg (the first row of left part in Fig. 4), the probability of choosing the lower left leg as exit leg is $b_1/4h_q$, the probability of choosing the lower right leg as exit leg is 0, the probability of choosing the upper left leg as exit leg is $a/4h_q$ and the probability of choosing the upper right leg as exit leg is $b/4h_q$. The summation of the four probabilities is 1. It is the same for other directed-loop segments and only the bare weights and weights in the extended space are different.

The solution of this set of equations is

$$b_1 = h_q, \quad b_2 = 0, \quad b_3 = 0, \\ a = 3h_q, \quad b = 0, \quad c = 0. \quad (16)$$

The right assignments give the second set of equations,

$$3h_q = b'_1 + a' + b', \\ 0 = a' + b'_2 + c', \\ 2h_q = b' + c' + b'_3. \quad (17)$$

The solution can be

$$b'_1 = h_q, \quad b'_2 = 0, \quad b'_3 = 0, \\ a' = 0, \quad b' = 2h_q, \quad c' = 0. \quad (18)$$

Secondly, the two sets of equations for the second and third columns in Fig. 3, where the right vertices are Γ_2 and Γ_3 respectively, are the same. The left assignments give a set of equations,

$$3h_q = b_1 + a + b, \quad 2h_q + \frac{1}{4} = a + b_2 + c, \\ \frac{1}{4} = b + c + b_3. \quad (19)$$

The solution is

$$\begin{aligned} \text{if } (h_q \leq \frac{1}{2}) \quad & b_1 = 0, \quad b_2 = 0, \quad b_3 = 0, \\ & a = \frac{5}{2}h_q, \quad b = \frac{h_q}{2}, \quad c = \frac{1}{4} - \frac{h_q}{2}, \\ \text{if } (h_q > \frac{1}{2}) \quad & b_1 = h_q - \frac{1}{2}, \quad b_2 = 0, \quad b_3 = 0, \\ & a = 2h_q + \frac{1}{4}, \quad b = \frac{1}{4}, \quad c = 0. \end{aligned} \quad (20)$$

The equations of the right assignment for these two columns are

$$\begin{aligned} 2h_q + \frac{1}{4} &= b'_1 + a' + b', \quad \frac{1}{4} = a' + b'_2 + c', \\ h_q &= b' + c' + b'_3. \end{aligned} \quad (21)$$

The solution can be

$$\begin{aligned} b'_1 &= h_q, \quad b'_2 = 0, \quad b'_3 = 0, \\ a' &= \frac{1}{4}, \quad b' = h_q, \quad c' = 0. \end{aligned} \quad (22)$$

Thirdly, the two sets of equations for the fourth and fifth columns in Fig. 3 are also the same, where the right vertices are Γ_4 and Γ_5 . The equations for the left set are

$$\begin{aligned} 0 &= b_1 + a + b, \quad \frac{1}{4} = a + b_2 + c, \\ \frac{1}{4} &= b + c + b_3. \end{aligned} \quad (23)$$

The solution can be

$$b_1 = 0, \quad b_2 = 0, \quad b_3 = 0, \quad a = 0, \quad b = 0, \quad c = \frac{1}{4}. \quad (24)$$

The equations of the right set are

$$\begin{aligned} \frac{1}{4} &= b'_1 + a' + b', \quad \frac{1}{4} = a' + b'_2 + c', \\ 0 &= b' + c' + b'_3. \end{aligned} \quad (25)$$

The solution can be

$$\begin{aligned} b'_1 &= 0, \quad b'_2 = 0, \quad b'_3 = 0, \\ a' &= \frac{1}{4}, \quad b' = 0, \quad c' = 0. \end{aligned} \quad (26)$$

At last, we give the two sets of equations for the sixth column in Fig. 3 and the right vertex is Γ_6 . The equations for the left set are

$$\begin{aligned} 2h_q &= b_1 + a + b, \quad h_q = a + b_2 + c, \\ 0 &= b + c + b_3. \end{aligned} \quad (27)$$

The solution can be

$$\begin{aligned} b_1 &= h_q, \quad b_2 = 0, \quad b_3 = 0, \\ a &= h_q, \quad b = 0, \quad c = 0. \end{aligned} \quad (28)$$

The right set equations are

$$\begin{aligned} h_q &= b'_1 + a' + b', \quad 0 = a' + b'_2 + c', \\ 0 &= b' + c' + b'_3. \end{aligned} \quad (29)$$

The solution can be

$$\begin{aligned} b'_1 &= h_q, \quad b'_2 = 0, \quad b'_3 = 0, \\ a' &= 0, \quad b' = 0, \quad c' = 0. \end{aligned} \quad (30)$$

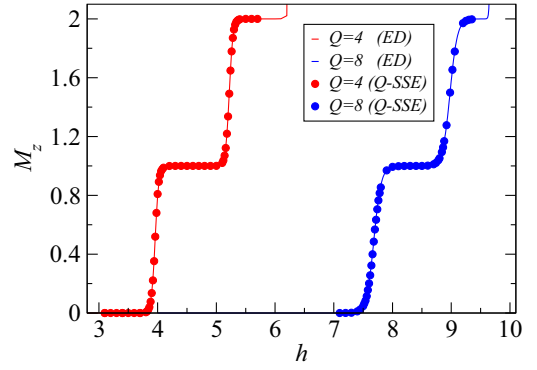


FIG. 5. Magnetization properties versus magnetic field for the JQ_2 model on square lattice. The lattice size is 4×4 and the inverse temperature is $\beta = 32$. The solid circles are results of the Q-SSE method and the solid lines are results of the ED method.

Based on these solutions, we can construct the directed-loop update. If we only use these solutions shown above, where the magnetic field is combined to the Q operators, we can get the Q-SSE method. However, if we not only use the above solutions but also use the solutions that the magnetic field are combined to the J operators, we can get the JQ-SSE. In this case, we need divide the magnetic field into two parts. One is put into the J operators and the second is put into the Q operators. In the next section, we will present the simulations results of the Q-SSE method and the JQ-SSE method.

VI. SIMULATIONS RESULTS

In this section, we present the simulation results of the Q-SSE and JQ-SSE methods. We will firstly show that the modified Q-SSE method is correct and the proof of correctness of the JQ-SSE method is shown in Appendix C. Then we compare the efficiency of the three different SSE methods.

A. Correctness of the Q-SSE method

In this subsection, we will prove the correctness of the Q-SSE method introduced above. As our modified program focuses on the properties of models with magnetic field, we mainly concentrate on the magnetization, which are defined as

$$M_z = \sum_{i=1}^N S_i^z. \quad (31)$$

In Fig. 5, we show the simulation results of the JQ_2 model on square lattice with $Q = 4$ and 8. The system size is 4×4 with inverse temperature $\beta = 32$. In this figure, the magnetization properties with magnetic field h for both the Q-SSE method and the ED method coincide. The results of these two different methods do agree with each other and it certifies the correctness of the Q-SSE method.

After proving the correctness of the Q-SSE method, we think the JQ-SSE method will also be right, which is just the combination of the J-SSE and Q-SSE method. In Appendix C, we present the results of the JQ-SSE method, which prove the correctness of the JQ-SSE method.

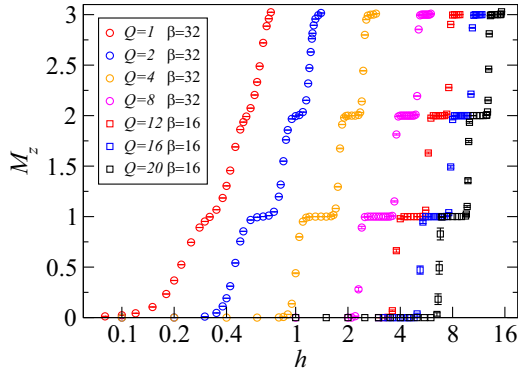


FIG. 6. Simulation results of the Q-SSE method on 16×16 square lattice at $\beta = 16$ or 32 .

B. Efficiency of the Q-SSE method

In this subsection, we focus on the efficiency of Q-SSE method. We firstly present the results of the Q-SSE method on 16×16 square lattice with $Q = 1, 2, 4, 8, 12, 16, 20$ at $\beta = 32$ or 16 in Fig. 6. The quality of magnetization curves is really good. The step structure of magnetization is really clear and the error bars are almost smaller than the symbol size. From this figure, we can see that we need larger external magnetic field to change the magnetization for larger Q interactions.

As mentioned earlier in this paper, the J-SSE method will become more and more worse when Q becomes larger as the autocorrelation time increases significantly. Figure 7 shows the simulation results of both the J-SSE and Q-SSE methods. We use the same Monte Carlo parameters for both methods (50 000 MCSs for equilibration, 50000×20 MCSs for measurement, we fix the number of loops in the directed-loop update in one MCS). As seen in Fig. 7(a), when Q is small ($Q = 2$), both the J-SSE method and the Q-SSE method give the correct results for magnetization for a low temperature $\beta = 32$. However, when $Q = 4$, we can find the results of the J-SSE method become worse, the fluctuations of data

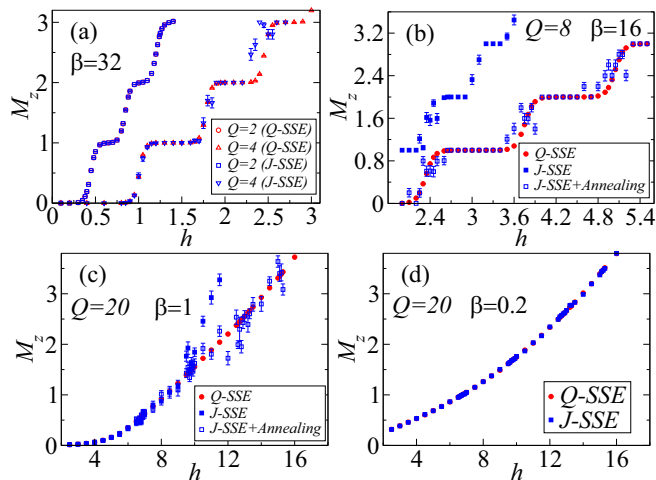


FIG. 7. Simulation results for magnetization vs external magnetic field with (a) $Q = 2, 4$ with $\beta = 32$; (b) $Q = 8$ with $\beta = 16$; (c) $Q = 20$ with $\beta = 1$; and (d) $Q = 20$ with $\beta = 0.2$.

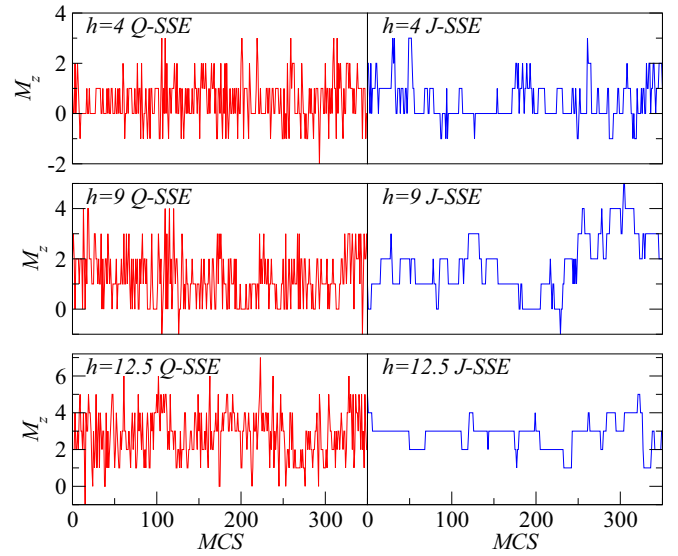


FIG. 8. Typical evolutions of magnetization for the JQ_2 model with $Q = 20$, $\beta = 0.2$. The magnetic fields are $h = 4, 9, 12.5$.

become larger, especially when $M_z > 2$. The quality of results for the Q-SSE method is still good enough. The results for $Q = 8$ at $\beta = 16$ are shown in Fig. 7(b). For this large value of Q , even the β become small, the J-SSE method gives incorrect results in our simulations. It is because the autocorrelation time is really large for the J-SSE method, the independent configurations change very slowly. For finite MCSs, the configurations may not be thermalized or we can not get enough independent configurations if we start with a thermalized configuration. Of course we can use other optimization methods in the J-SSE method to improve the results, such as the replica exchange method and the annealing method [16,17]. In this paper, we adopt the annealing method in the J-SSE method, which slowly reduces the temperature. We denote this method as “J-SSE+Annealing”. After annealing, the magnetizations give the right results. But the error bars are still large. However, the quality of the results in Q-SSE method is as good as that of small Q . In Fig. 7(c), we present the results for $Q = 20$ at $\beta = 1$. The value of Q is really large and the temperature is really high. However, even for this high temperature, the results of the J-SSE method only keep correct for small magnetic field h . While the results for large field are still incorrect. After applied the annealing technique, the results will be right but the error bars are also very large. If we raise the model to a much more higher temperature $\beta = 0.2$, the results of the J-SSE method are finally correct for all calculated magnetic fields, as shown in Fig. 7(d).

From Fig. 7, we can clearly see that the general J-SSE method will fail for large Q and low temperature with finite MCSs. In order to elucidate this conclusion in more detail, we present the typical evolutions for both the J-SSE method and the Q-SSE method in Fig. 8. We also present the autocorrelation properties later. Figure 8 shows the typical evolutions of magnetization with 350 MCSs for both the J-SSE method and the Q-SSE method at $Q = 20$ on 16×16 square lattice. The inverse temperature chosen in this figure is $\beta = 0.2$. We choose three different magnetic fields $h = 4, 9, 12.5$ and the

expectation values of the magnetization for these fields are around 0.5, 1.5, 2.5 respectively [it can be seen in Fig. 7(d)]. We can clearly see that the evolutions of magnetization is faster in the Q-SSE method than that in the J-SSE method. When the external field increases, the evolution in the J-SSE method will become even slower and it seems the evolution speed in the Q-SSE method changes very little. In this part, we have not shown the efficiency of the JQ-SSE method. It will be presented in the next section via the autocorrelation times.

C. Autocorrelations

The autocorrelation functions provide direct quantitative measurement of the efficiency of a Monte Carlo method in generating the independent configurations. In this part, we will focus on the autocorrelations. For a quantity O , the normalized autocorrelation function is defined as

$$A_O(t) = \frac{\langle O(i+t)O(i) \rangle - \langle O(i) \rangle^2}{\langle O(i)^2 \rangle - \langle O(i) \rangle^2} \quad (32)$$

where i and t are Monte Carlo times (we use the unit of 1 MCS). The brackets indicate the average over time i . For large time separations, the autocorrelation function decays exponentially as

$$A(t) \xrightarrow{t \rightarrow \infty} a e^{-t/\tau_{\text{exp}}}, \quad (33)$$

τ_{exp} is the exponential autocorrelation time and a is a constant. This time is given by the slowest mode of the simulation to which the observable O couples. At smaller time, usually other modes contribute and $O(t)$ behaves no longer purely exponentially.

Here we also introduce another time: the integrated autocorrelation time, which is defined as

$$\tau_{\text{int}}[O] = 1/2 + \sum_{t=1}^{\infty} A_O(t). \quad (34)$$

This time is the autocorrelation measure of the greatest practical utility [18]. In general, these two times are different. Only if $A(t)$ is a pure exponential, the two times coincide. In this paper, we focus on the autocorrelations of magnetizations.

In this part, we not only pay attention to the autocorrelations of magnetizations in the J-SSE and Q-SSE methods, we also study the autocorrelations in the JQ-SSE method. In the JQ-SSE method, as mentioned above, the external magnetic field should be divided into two parts and be combined with J interactions (Heisenberg interactions) and Q interactions respectively. The directed-loop updates will be carried out on both the J and Q bonds. In this method, there is another freedom: the division ratio. For a magnetic field h on a spin, we can divide it into two magnetic fields. We denote the strength of the first field as h_j and this field will be combined to the J interactions. The strength of the second field, which will be put into the Q interactions, is $h - h_j$. The value of h_j should be $0 \leq h_j \leq h$. We define the division ratio of the magnetic field as h_j/h , which is the ratio of magnetic field that will be applied to the J interactions. The J-SSE and Q-SSE methods are two extreme cases: $h_j/h = 1$ for the J-SSE method, $h_j/h = 0$ for the Q-SSE method.

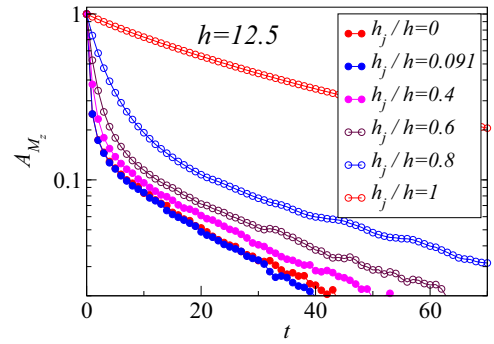


FIG. 9. The normalized autocorrelation function for $Q = 20$, $h = 12.5$, and $\beta = 0.2$ on 16×16 square lattice.

We firstly present the normalized autocorrelation function at $Q = 20$, $h = 12.5$, $\beta = 0.2$ on 16×16 square lattice in Fig. 9. We can clearly find when $h_j/h = 1$ (J-SSE method), the autocorrelation function is the largest. The ratio of the smallest autocorrelation function is close to 0 (we can not determine the exact ratio).

Next in Fig. 10, we present the magnetization integrated autocorrelation time for $Q = 1, 2, 4, 8, 12, 16, 20$ and the exponential autocorrelation time for $Q = 20$. The integrated autocorrelation times are calculated from Eq. (34) and we fit the exponential autocorrelation time from autocorrelation functions based on Eq. (33). In this figure, we choose different temperatures for different Q . That is because we need ensure the JQ-SSE methods in all division ratios give the right results in our finite MCSs (we have verified the results for all ratios are correct). In addition, we choose three different magnetic fields for every Q , in which the expectation values of magnetization are around 0.5, 1, 1.5 respectively. From Fig. 10, we can find that the autocorrelation times are the biggest for

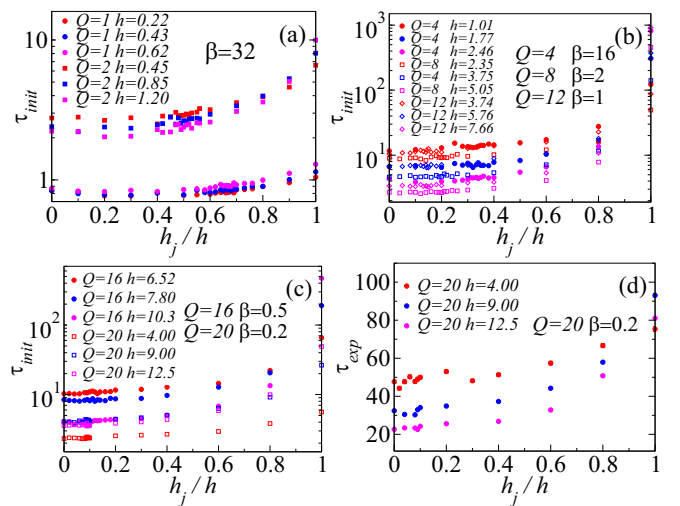


FIG. 10. Integrated autocorrelation time and exponential autocorrelation time of magnetizations versus the division ratio of magnetic field in the JQ-SSE method for JQ_2 model on 16×6 square lattice. [(a)–(c)] The integrated autocorrelation for $Q = 1, 2, 4, 8, 12, 16, 20$. (d) The exponential autocorrelation time for $Q = 20$.

$h_j/h = 1$ (J-SSE method) even for $Q = 1$ and 2 . When Q increases, the autocorrelation times increase significantly at $h_j/h = 1$. It means the J-SSE method is the worst choice to do the simulations of the JQ_2 model with magnetic field for these values of Q (Of course, we can argue that when Q is much smaller, the J-SSE method is the best choice). Although the autocorrelation for J-SSE method is the largest for small Q , the autocorrelation times for the J-SSE method are still not large ($\tau_{\text{init}} < 10$ for $Q = 1, 2$). So the simulations of the J-SSE method for small Q are still good enough. For large Q , the smallest autocorrelation times seem to be close to $h_j/h = 0$. In addition, for a large range of the ratio around 0, the autocorrelation times do not change too much. We can not clearly find the best ratio for large Q in this figure. So we suggest that the Q-SSE method is good enough for simulating the JQ_2 model with large Q . We do not need to optimize the ratio in the JQ-SSE method to find the smallest autocorrelation time, which is very close to that of $h_j/h = 0$. The results shown in Fig. 10 are based on $(5 - 10) \times 10^5$ MCSs for each data point.

VII. SUMMARY

In this paper, we argue that if we study the JQ_2 model with external magnetic field, the general SSE method with directed loops (J-SSE method) will be good enough for small Q interactions. However, when the Q interactions become large and the temperature is low, this general SSE method may fail with finite MCSs. Here we introduce the modified SSE methods (the Q-SSE and JQ-SSE methods) to deal with this problem. These modified methods can really decrease the autocorrelation times especially for large Q interactions. Thus it can really speed up the simulations. In addition, we argue that when doing simulations of the JQ_2 model with large Q , the Q-SSE method is good enough. We do not need to optimize the ratio h_j/h to find the smallest autocorrelation time in the JQ-SSE method, which is very close to that of the Q-SSE method.

The principle behind these modified methods is that for the JQ_2 model, the products of operators in the SSE configurations S_M not only contain the J operators but also have the Q operators. The general J-SSE method only make use of the J operators to do the directed-loop updates. When Q becomes large, the portion of the J operators in the operator products will be very small. It means the general method only affect really small part of the products. The methods introduced here, consider the main part of the operators (Q-SSE method) or even all the part of products (JQ-SSE method), which are much better than the general J-SSE method.

Such methods and idea can be applied to other models, such the JQ_3 model and the $CBJQ$ model. If there are N types of interactions, we can also divide the magnetic field into N parts and combine them with every type of interactions respectively. These methods will certainly speed up the simulations of these models.

In this article, we have not paid attention to the effect of the constant added to the Hamiltonian and the different solutions to the directed loop-equations. The three SSE methods all choose the smallest constant and minimize the bounce probability. We focus on the efficiency difference when combining the magnetic fields with different types of operators. The

two treatments of the magnetic field improve the efficiency significantly.

ACKNOWLEDGMENTS

This work is supported by Beijing Institute of Technology Research Fund Program for Young Scholars and the National Natural Science Foundation of China under Grant No. 12304171.

APPENDIX A: SOLUTIONS OF THE DIRECTED-LOOP EQUATIONS

In this Appendix, we will present how to solve the directed-loop equations in Eqs. (15), (17), (19), (21), (23), (25), (27), and (29) step-by-step. The solution for the general form of directed-loop equations has been discussed in Ref. [4]. In the JQ_2 model, there are three equations in every set. It is convenient to label three weights as W_1, W_2, W_3 and $W_3 \geq W_2 \geq W_1$. The weights in every set can be relabeled in this order and every set of equations can be written as

$$\begin{aligned} W_1 &= a_{11} + a_{12} + a_{13}, \\ W_2 &= a_{21} + a_{22} + a_{23}, \\ W_3 &= a_{31} + a_{32} + a_{33}, \end{aligned} \quad (\text{A1})$$

where all a_{ij} should be non-negative and $a_{ij} = a_{ji}$. The bounce probabilities are determined by $a_{ii}, i = 1, 2, 3$. As we want to minimize the bounce probabilities, we can set $a_{ii} = 0$ for $i = 1, 2, 3$. Then there are three independent unknowns (a_{12}, a_{13}, a_{23}) and three equations, which make the solution unique. However, every a_{ij} should be non-negative and we can find only when $W_3 \leq W_1 + W_2$, all the three a_{ii} can be 0. In this condition, the solution is

$$\begin{aligned} a_{12} &= a_{21} = (W_1 + W_2 - W_3)/2, \\ a_{13} &= a_{31} = (W_1 - W_2 + W_3)/2, \\ a_{23} &= a_{32} = (-W_1 + W_2 + W_3)/2. \end{aligned} \quad (\text{A2})$$

When $W_3 > W_1 + W_2$, we can always permit one bounce probabilities not be zero (this is the bounce in the largest weight W_3 configuration). We set $a_{11} = a_{22} = 0$ and $a_{33} = W_3 - W_1 - W_2$ and the solution for the three unknowns is

$$\begin{aligned} a_{12} &= a_{21} = 0, \quad a_{13} = a_{31} = W_1, \\ a_{23} &= a_{32} = W_2. \end{aligned} \quad (\text{A3})$$

Based on Eqs. (A2) and (A3), we now solve the eight independent sets of equations for the JQ_2 model with magnetic field.

The weights of the first set of equations [Eqs. (15)] are $W_1 = 0, W_2 = 3h_q, W_3 = 4h_q$ (we have relabeled the order of the weight). As $W_1 + W_2 < W_3$, we can get the solution according to Eqs. (A3),

$$\begin{aligned} a_{11} &= a_{22} = 0, \\ a_{33} &= W_3 - W_1 - W_2 = h_q, \\ a_{12} &= a_{21} = 0, \\ a_{13} &= a_{31} = W_1 = 0, \\ a_{23} &= a_{32} = W_2 = 3h_q. \end{aligned} \quad (\text{A4})$$

This is just the solution shown in Eqs. (16).

The weights of the second set of equations [Eqs. (17)] are $W_1 = 0$, $W_2 = 2h_q$, $W_3 = 3h_q$. As $W_1 + W_2 < W_3$, we get the solution according to Eqs. (A3),

$$\begin{aligned} a_{11} &= a_{22} = 0, \\ a_{33} &= W_3 - W_1 - W_2 = h_q, \\ a_{12} &= a_{21} = 0, \\ a_{13} &= a_{31} = W_1 = 0, \\ a_{23} &= a_{32} = W_2 = 2h_q. \end{aligned} \quad (\text{A5})$$

This is just the solution shown in Eqs. (18).

The weights of the third set of equations [Eqs. (19)] are $3h_q$, $2h_q + 1/4$, $1/4$. The order of the weight depends on the value of h_q . When $h_q \leq 1/12$, $W_1 = 3h_q$, $W_2 = 1/4$, $W_3 = 2h_q + 1/4$. As $W_1 + W_2 \geq W_3$, we get the solution according to Eqs. (A2),

$$\begin{aligned} a_{11} &= a_{22} = a_{33} = 0, \\ a_{12} &= a_{21} = (W_1 + W_2 - W_3)/2 = h_q/2, \\ a_{13} &= a_{31} = (W_1 - W_2 + W_3)/2 = 5h_q/2, \\ a_{23} &= a_{32} = (-W_1 + W_2 + W_3)/2 = 1/4 - h_q/2. \end{aligned} \quad (\text{A6})$$

When $1/12 \leq h_q \leq 1/4$, $W_1 = 1/4$, $W_2 = 3h_q$, $W_3 = 2h_q + 1/4$. As $W_1 + W_2 \geq W_3$, we get the solution according to Eqs. (A2),

$$\begin{aligned} a_{11} &= a_{22} = a_{33} = 0, \\ a_{12} &= a_{21} = (W_1 + W_2 - W_3)/2 = h_q/2, \\ a_{13} &= a_{31} = (W_1 - W_2 + W_3)/2 = 1/4 - h_q/2, \\ a_{23} &= a_{32} = (-W_1 + W_2 + W_3)/2 = 5h_q/2, \end{aligned} \quad (\text{A7})$$

When $1/4 < h_q \leq 1/2$, $W_1 = 1/4$, $W_2 = 2h_q + 1/4$, $W_3 = 3h_q$. As $W_1 + W_2 \geq W_3$, we get the solution according to Eqs. (A2),

$$\begin{aligned} a_{11} &= a_{22} = a_{33} = 0, \\ a_{12} &= a_{21} = (W_1 + W_2 - W_3)/2 = 1/4 - h_q/2, \\ a_{13} &= a_{31} = (W_1 - W_2 + W_3)/2 = h_q/2, \\ a_{23} &= a_{32} = (-W_1 + W_2 + W_3)/2 = 5h_q/2. \end{aligned} \quad (\text{A8})$$

When $h_q > 1/2$, $W_1 = 1/4$, $W_2 = 2h_q + 1/4$, $W_3 = 3h_q$. As $W_1 + W_2 < W_3$, we get the solution according to Eqs. (A3),

$$\begin{aligned} a_{11} &= a_{22} = 0, \\ a_{33} &= W_3 - W_1 - W_2 = h_q - 1/2, \\ a_{12} &= a_{21} = 0, \\ a_{13} &= a_{31} = W_1 = 1/4, \\ a_{23} &= a_{32} = W_2 = 2h_q + 1/4. \end{aligned} \quad (\text{A9})$$

There are four solutions for the third set of equations under different conditions. But one can find that Eqs. (A7)–(A9) give the same solution. That is because under these three conditions, the weights all have the property $W_1 + W_2 \geq W_3$, which means $a_{ii} = 0$. Thus the solution of the unknown is unique. We set $W_1 = 1/4$, $W_2 = 2h_q + 1/4$, $W_3 = 3h_q$ and summarize

the solutions for Eqs. (19): when $h_q \leq 1/2$,

$$\begin{aligned} a_{11} &= a_{22} = a_{33} = 0, \\ a_{12} &= a_{21} = 1/4 - h_q/2, \\ a_{13} &= a_{31} = h_q/2, \\ a_{23} &= a_{32} = 5h_q/2, \end{aligned}$$

when $h_q > 1/2$,

$$\begin{aligned} a_{11} &= a_{22} = 0, \\ a_{33} &= h_q - 1/2, \\ a_{12} &= a_{21} = 0, \\ a_{13} &= a_{31} = 1/4, \\ a_{23} &= a_{32} = 2h_q + 1/4. \end{aligned} \quad (\text{A10})$$

This is just the solution shown in Eqs. (20).

The weights of the fourth set of equations [Eqs. (21)] are $W_1 = h_q(1/4)$, $W_2 = 1/4(h_q)$, $W_3 = 2h_q + 1/4$ when $h_q \leq 1/4$ ($h_q > 1/4$). As $W_1 + W_2 < W_3$, we get the solution according to Eqs. (A3). The value of h_q only changes the order of W_1 and W_2 , which does not change the solution. We can present the solutions together. We set $W_1 = h_q$, $W_2 = 1/4$, $W_3 = 2h_q + 1/4$, the solution for this set of equation is

$$\begin{aligned} a_{11} &= a_{22} = 0, \\ a_{33} &= W_3 - W_1 - W_2 = h_q, \\ a_{12} &= a_{21} = 0, \\ a_{13} &= a_{31} = W_1 = h_q, \\ a_{23} &= a_{32} = W_2 = 1/4. \end{aligned} \quad (\text{A11})$$

This is just the solution shown in Eqs. (22).

The weights of the fifth and sixth sets of equations [Eqs. (23) and (25)] are same: $W_1 = 0$, $W_2 = 1/4$, $W_3 = 1/4$. As $W_1 + W_2 \geq W_3$, we get the solution according to Eqs. (A2),

$$\begin{aligned} a_{11} &= a_{22} = a_{33} = 0, \\ a_{12} &= a_{21} = (W_1 + W_2 - W_3)/2 = 0, \\ a_{13} &= a_{31} = (W_1 - W_2 + W_3)/2 = 0, \\ a_{23} &= a_{32} = (-W_1 + W_2 + W_3)/2 = 1/4. \end{aligned} \quad (\text{A12})$$

This is just the solution shown in Eqs. (24) and (26).

The weights of the seventh set of equations [Eqs. (27)] are $W_1 = 0$, $W_2 = h_q$, $W_3 = 2h_q$. As $W_1 + W_2 < W_3$, we get the solution according to Eqs. (A3),

$$\begin{aligned} a_{11} &= a_{22} = 0, \\ a_{33} &= W_3 - W_1 - W_2 = h_q, \\ a_{12} &= a_{21} = 0, \\ a_{13} &= a_{31} = W_1 = 0, \\ a_{23} &= a_{32} = W_2 = h_q. \end{aligned} \quad (\text{A13})$$

This is just the solution shown in Eqs. (28).

The weights of the eighth set of equations [Eqs. (29)] are $W_1 = 0$, $W_2 = 0$, $W_3 = h_q$. As $W_1 + W_2 < W_3$, we get the

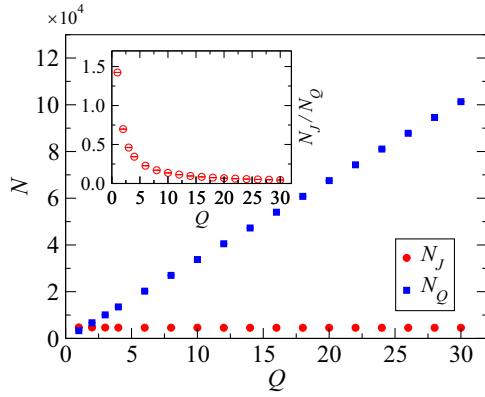


FIG. 11. The number of the J bonds (N_J) and the Q bonds (N_Q) in SSE configurations of the JQ_2 model without external field. The system size is $L = 16$ and the inverse temperature is $\beta = 16$. The inset shows the ratio of the number of J bonds to the number of Q bonds.

solution according to Eqs. (A3),

$$\begin{aligned}
 a_{11} &= a_{22} = 0, \\
 a_{33} &= W_3 - W_1 - W_2 = h_q, \\
 a_{12} &= a_{21} = 0, \\
 a_{13} &= a_{31} = W_1 = 0, \\
 a_{23} &= a_{32} = W_2 = 0,
 \end{aligned} \tag{A14}$$

This is just the last solution shown in Eqs. (30).

APPENDIX B: THE NUMBER OF THE J AND Q BONDS IN THE JQ_2 MODEL

As mentioned in main text, the Q bonds will appear more frequently than the J bonds in the JQ_2 model, when Q is large. In Fig. 11, we present simulation results to verify such statement. We perform SSE simulations to study the properties of the number of the J bonds and the Q bonds appearing in the SSE configurations in the JQ_2 model without external field. The system is $L = 16$ square lattice and the inverse temperature is $\beta = 16$. The strength of the J bonds is set to 1 and the strength of Q bonds ranges from 1 to 30. One can find that when the value of Q increases, the number of the J bonds will decrease very slowly and the number of the Q bonds will increase very fast. The inset in Fig. 11 shows the ratio of the number of J bonds to the number of Q bonds. The ratio will decrease to very small value when Q is very large.

APPENDIX C: RESULTS FOR THE JQ-SSE METHOD

In this Appendix, we present the simulation results for the JQ_2 model at $Q = 8$ with external magnetic field by the JQ-SSE method. The inverse temperature is $\beta = 16$ and the system size is $L = 16$. h_j/h is the ratio of magnetic field that is applied to the J bonds. We use 50 000 MCSs for equilibrium, 50000×20 MCSs for measurement for all h_j/h . When $h_j/h = 1$, it is just the J-SSE method, which has the largest autocorrelation time. The MCSs used here are not

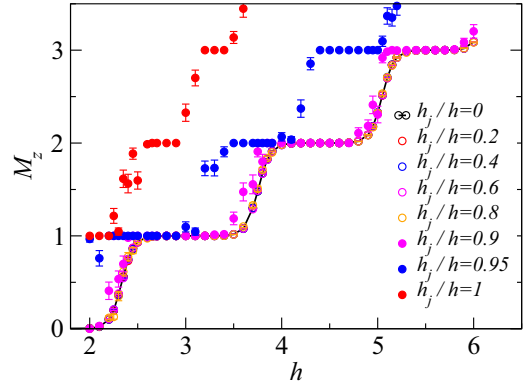


FIG. 12. Simulation results for magnetization versus external magnetic field with $Q = 8$ at $\beta = 16$. h_j/h is the ratio of magnetic field applied into J bonds.

large enough to give the right answer. When $h_j/h = 0$, it's the Q-SSE method. We think it gives the right results in our simulations, as we have proven its correctness in main text. In Fig. 12, one can find when the ratio $h_j/h \leq 0.8$, the magnetization curves are the same as that of $h_j/h = 0$, which means the JQ-SSE method is right. However, when h_j/h is close to 1, the results diverge from the correct results. The reason is that for ratio close to 1, the JQ-SSE method is close to the J-SSE method and the most part of magnetic field is still applied into the J bonds. Although the autocorrelation time decreases as the ratio reduces, the autocorrelation times are still large compared to our MCSs. In addition, even for $h_j/h = 0.9$, which is close to the J-SSE method, the results are very close to the right results.

APPENDIX D: RESULTS FOR THE Q-SSE METHOD AT LARGE Q

In this Appendix, we present simulation results (Fig. 13) for even large Q strength ($Q = 30$) at $\beta = 16, 32$ via the Q-SSE method. We can clearly see the step structure of magnetization.

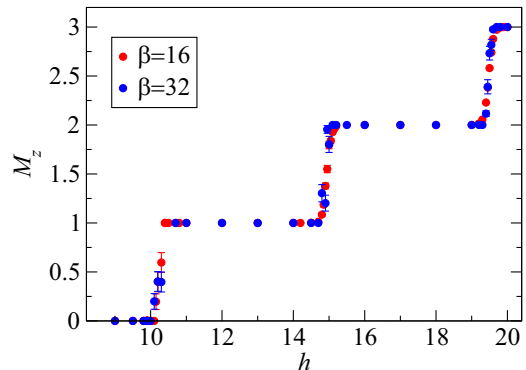


FIG. 13. Simulation results for magnetization versus external magnetic field with $Q = 30$ at $\beta = 16, 32$.

- [1] A. W. Sandvik and J. Kurkijärvi, Quantum Monte Carlo simulation method for spin systems, *Phys. Rev. B* **43**, 5950 (1991).
- [2] A. W. Sandvik, Stochastic series expansion method with operator-loop update, *Phys. Rev. B* **59**, R14157 (1999).
- [3] A. W. Sandvik, Computational studies of quantum spin systems, *AIP Conf. Proc.* **1297**, 135 (2010).
- [4] O. F. Syljuåsen and A. W. Sandvik, Quantum Monte Carlo with directed loops, *Phys. Rev. E* **66**, 046701 (2002).
- [5] A. Iaizzi, K. Damle, and A. W. Sandvik, Field-driven quantum phase transitions in $S = 1/2$ spin chains, *Phys. Rev. B* **95**, 174436 (2017).
- [6] A. Iaizzi, K. Damle, and A. W. Sandvik, Metamagnetism and zero-scale-factor universality in the two-dimensional J - Q model, *Phys. Rev. B* **98**, 064405 (2018).
- [7] Y. Cui, L. Liu, H. Lin, K.-H. Wu, W. Hong, X. Liu, C. Li, Z. Hu, N. Xi, S. Li *et al.*, Proximate deconfined quantum critical point in $\text{SrCu}_2(\text{BO}_3)_2$, *Science* **380**, 1179 (2023).
- [8] A. W. Sandvik, Evidence for deconfined quantum criticality in a two-dimensional Heisenberg model with four-spin interactions, *Phys. Rev. Lett.* **98**, 227202 (2007).
- [9] J. Lou, A. W. Sandvik, and N. Kawashima, Antiferromagnetic to valence-bond-solid transitions in two-dimensional $\text{SU}(N)$ Heisenberg models with multispin interactions, *Phys. Rev. B* **80**, 180414(R) (2009).
- [10] B. Zhao, P. Weinberg, and A. W. Sandvik, Symmetry-enhanced discontinuous phase transition in a two-dimensional quantum magnet, *Nat. Phys.* **15**, 678 (2019).
- [11] J. Takahashi and A. W. Sandvik, Valence-bond solids, vestigial order, and emergent $\text{SO}(5)$ symmetry in a two-dimensional quantum magnet, *Phys. Rev. Res.* **2**, 033459 (2020).
- [12] B. Zhao, J. Takahashi, and A. W. Sandvik, Multicritical deconfined quantum criticality and Lifshitz point of a helical valence-bond phase, *Phys. Rev. Lett.* **125**, 257204 (2020).
- [13] H. Shao, Wenan Guo, and A. W. Sandvik, Quantum criticality with two length scales, *Science* **352**, 213 (2016).
- [14] A. W. Sandvik, A generalization of Handscomb's quantum Monte Carlo scheme-application to the 1D Hubbard model, *J. Phys. A* **25**, 3667 (1992).
- [15] A. Dorneich and M. Troyer, Accessing the dynamics of large many-particle systems using the stochastic series expansion, *Phys. Rev. E* **64**, 066701 (2001).
- [16] K. Hukushima and K. Nemoto, Exchange Monte Carlo method and application to spin glass simulations, *J. Phys. Soc. Jpn.* **65**, 1604 (1996).
- [17] S. Kirkpatrick, C. D. Gelatt, and M. P. Vecchi, Optimization by simulated annealing, *Science* **220**, 671 (1983).
- [18] *Computational Many-Particle Physics*, edited by H. Fehske, R. Schneider, and A. Weiße, Lecture Notes in Physics Vol. 739 (Springer, Berlin, 2008).